

Exceptional field dependence of antiferromagnetic magnons in LiFePO₄

J. Werner,¹ C. Neef,^{1,2} C. Koo,¹ A. Ponomaryov,³ S. Zvyagin,³ and R. Klingeler^{1,4,*}

¹*Kirchhoff Institute of Physics, Heidelberg University, INF 227, D-69120 Heidelberg, Germany*

²*Fraunhofer Institute for Systems and Innovation Research ISI, Karlsruhe D-76139, Germany*

³*Dresden High Magnetic Field Laboratory (HLD-EMFL),*

Helmholtz-Zentrum Dresden Rossendorf, D-01328 Dresden, Germany

⁴*Centre for Advanced Materials (CAM), Heidelberg University, INF 225, D-69120 Heidelberg, Germany*

(Dated: April 28, 2021)

Low-energy magnon excitations in magnetoelectric LiFePO₄ have been investigated by high-frequency high-field electron spin resonance spectroscopy in magnetic fields up to $B = 58$ T and frequencies up to $f = 745$ GHz. For magnetic fields applied along the easy magnetic axis, the excitation gap softens and vanishes at the spin-flop field of $B_{\text{SF}} = 32$ T before hardening again at higher fields. In addition, for $B \lesssim B_{\text{SF}}$ we observe a resonance mode assigned to excitations due to Dzyaloshinskii-Moriya (DM)-interactions, thereby evidencing sizable DM interaction of $\approx 150 \mu\text{eV}$ in LiFePO₄. Both the magnetisation and the excitations up to high magnetic fields are described in terms of a mean-field theory model which extends recent zero field inelastic neutron scattering results. Our results imply that magnetic interactions as well as magnetic anisotropy have a sizeable quadratic field dependence which we attribute to significant magnetostriction.

PACS numbers:

I. INTRODUCTION

There is a variety of experimental techniques to probe and elucidate spin dynamics in magnetically ordered materials, among them inelastic neutron scattering (INS), resonant inelastic X-ray scattering (RIXS), Raman- and terahertz spectroscopy, or high-frequency electron spin resonance spectroscopy (HF-ESR). While probing the same low-temperature magnetic excitations aiming at establishing the magnetic Hamiltonian for a material, the experiments are complementing each other as, e.g., different sample size, resolution, energy and reciprocal space regimes, or magnetic fields are accessible. One illustrative example is BiFeO₃ where INS¹⁻³, terahertz-spectroscopy⁴⁻⁶, HF-ESR⁷ and Raman^{8,9} data have lead to a conclusive view and established the microscopic spin Hamiltonian. Our current work on LiFePO₄ highlights not only the strength of antiferromagnetic resonance (AFMR) studies to probe low-energy magnetic excitations but also illustrates how microscopic parameters can change upon application of high magnetic fields, e.g., by magnetostrictive effects.

Due to intriguing magnetoelectric properties¹⁰⁻¹⁵, spin excitations in olivine-type lithium orthophosphates LiMPO₄ ($M = \text{Mn, Fe, Co, Ni}$) have been measured by various experiments. While for LiMnPO₄ and LiNiPO₄, complementing investigations by INS, THz- and Raman-spectroscopy enabled to establishing microscopic spin models, for LiCoPO₄ and LiFePO₄ comprehensive models are, however, still missing. Among the above mentioned olivine-type phosphates, LiMnPO₄ shows the smallest magnetocrystalline anisotropy as probed by ESR in the paramagnetic phase and around the antiferromagnetic (AFM) ordering temperature¹⁶. Inelastic neutron scattering revealed accordingly small magnon excitation gaps of $\Delta_1 \approx 120$ GHz and $\Delta_2 \approx 160$ GHz in the ordered phase¹⁷. Raman data corroborated a microscopic spin model which together with INS results led to a robust set of magnetic parameters¹⁸. A similar picture evolves for LiNiPO₄ from Raman and INS data where low energy spin excitation gaps of $\Delta_1 \approx 450$ GHz and $\Delta_2 \approx 1.1$ THz were found¹⁹⁻²². Infrared absorption spectroscopy confirm the INS results²³ and recent Raman scattering results provide an independent experimental confirmation of previously obtained exchange parameters²⁴. In contrast, a conclusive model for LiCoPO₄ is still under debate which might be due to the strong magnetoelectric effect in this material¹¹. Spin excitations in LiCoPO₄ have been studied extensively both by INS²⁵⁻²⁷ and infrared-absorption spectroscopy^{28,29}. It was revealed that the excitation gaps in the center of the Brillouin zone are $\Delta_1 \approx 1.1$ THz and $\Delta_2 \approx 1.3$ THz. Here, we report on LiFePO₄ where previous investigations of low energy spin excitations have been performed by Raman spectroscopy³⁰ and INS^{15,31,32}. The zero-field spin configuration based on Refs. 15 and 32 is shown in Fig. 1. While the magnetic moments are pointing mainly along the crystallographic b -axis, there is also a small canting which indicates the presence of Dzyaloshinsky-Moriya interaction¹⁵. The INS reports agree that the relevant exchange interactions are all antiferromagnetic and that the dominant interaction is J_{bc} (see Fig. 1) but the exact values differ significantly.⁴⁶ Furthermore, the INS results can not explain the static magnetic properties in magnetic fields at low-temperature, as a spin-flop-like transition at $B_{\text{SF}} = 32$ T is not reproduced by the INS model.

To clarify these issues and to investigate the spin-flop transition in more detail we performed high-frequency/high-field electron spin resonance spectroscopy (HF-ESR) studies on LiFePO₄. Our study reveals the presence of low-energy magnon modes around the spin-flop field. Both the softening of these magnon modes towards B_{SF} and the

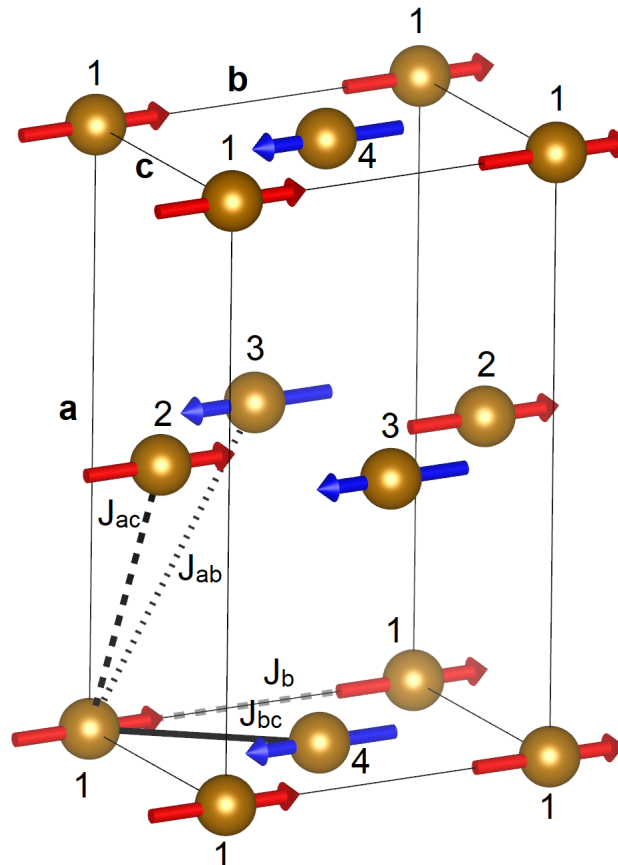


FIG. 1: Schematic view of magnetic structure of LiFePO_4 at zero field, based on Refs. 15 and 32. Numbers illustrate how the Fe-moments are associated with four antiferromagnetic sublattices. J_{ab} , J_{ac} , J_{bc} , and J_b are the leading magnetic interactions. The figure has been generated with VESTA³³.

magnetisation are described by means of a mean-field theory model which, while based on the INS model, employs field dependent values of magnetic interaction and magnetic anisotropy. In addition, we find direct evidence for finite DM interactions. The estimated size of the DM interaction is $150\mu\text{eV}$. Measurements at higher temperatures reveal the disappearance of the resonances already well below the antiferromagnetic ordering temperature.

II. EXPERIMENTAL

Single crystals of LiFePO_4 were grown by the high-pressure optical floating-zone method as reported in detail in Ref. [34]. High-frequency electron spin resonance spectroscopy (HF-ESR) experiments in pulsed fields up to 50 T and magnetization studies up to 58 T were performed at the Dresden High Magnetic Field Laboratory (HLD). The HF-ESR data were obtained using VDI modular transmitters (product of Virginia Diodes Inc., USA) as sub-mm radiation sources and InSb hot-electron bolometer as a radiation detector. The experiments have been performed at frequencies f between 65 and 1100 GHz. However, at $750\text{ GHz} \leq f \leq 1100\text{ GHz}$, there is strong magnetic field-independent microwave absorption, possibly due to non-magnetic excitation, which does not allow to obtain reliable data in this frequency regime. Magnetization studies employed a coaxial pick-up coil system; the magnetization data were calibrated using data, obtained in static fields at 5 T (see Ref. [35]).

III. RESULTS

Long-range antiferromagnetic order in LiFePO_4 single crystals studied at hand³⁴ evolves at $T_N = 50.0(5)\text{ K}$ with the crystallographic b -axis being the magnetic easy axis. Magnetic fields applied along the magnetic easy axis of LiFePO_4

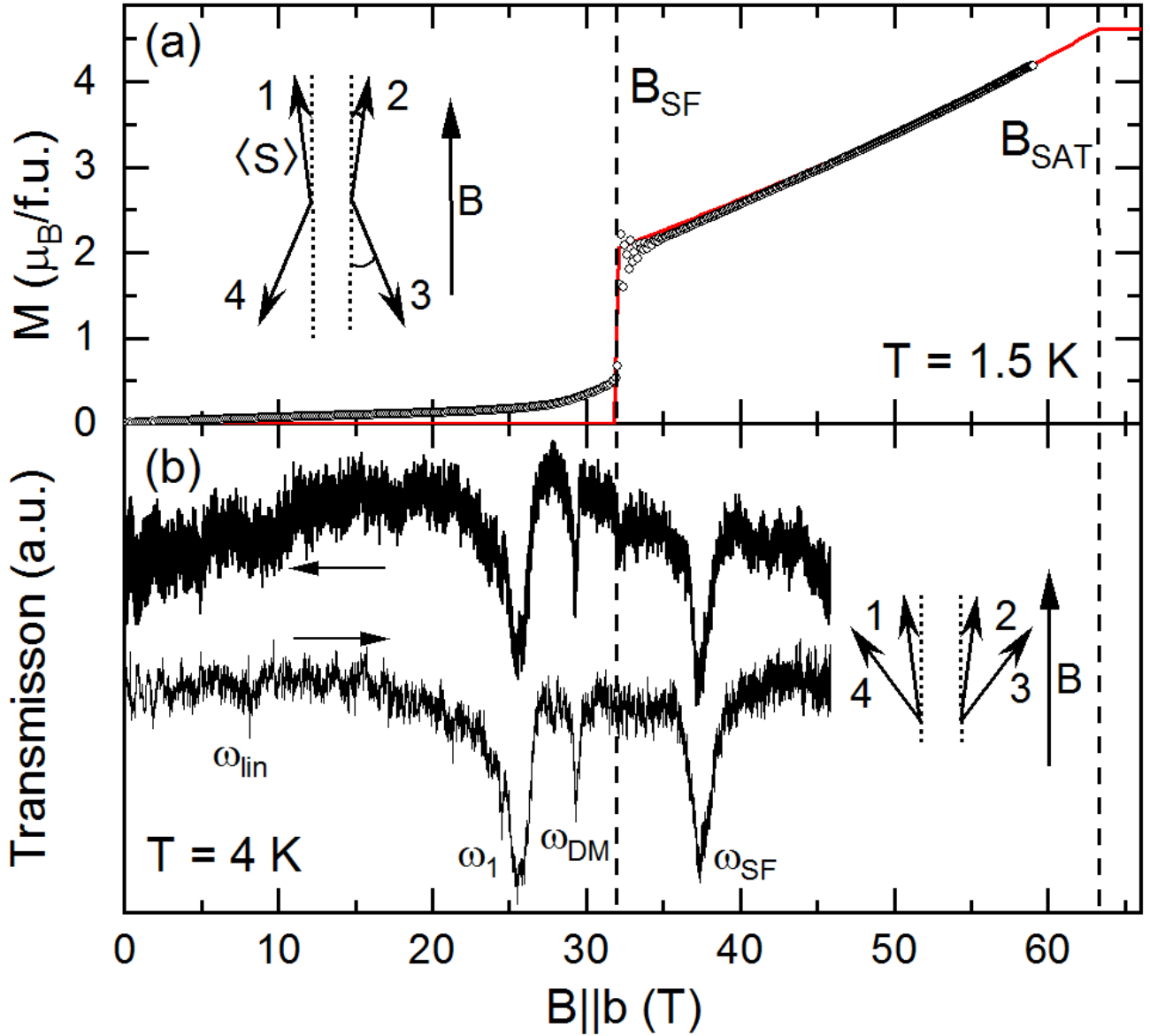


FIG. 2: (a) Pulsed-field magnetization of LiFePO₄ with $B||b$ at $T = 1.5$ K³⁵. Red line is a simulation of the data, see the text. Vertical dashed lines indicate the spin-flop field B_{SF} and the saturation field B_{sat} . (b) Pulsed-field electron spin resonance up-sweep (\rightarrow) and down-sweep (\leftarrow) spectra at $T = 4$ K and $f = 708$ GHz. The resonances are labeled with ω_{lin} for the linear resonance branch and $\omega_{1,DM,SF}$ (see Fig. 4). Pictograms indicate the magnetic structure respectively the model for $B||b$ (a) at $B < B_{SF}$ (adapted from Ref. 15), and (b) in the spin-flop phase.

leads to a jump in magnetization at around $B_{SF} = 32$ T and a rather linear behavior above the metamagnetic transition, see Fig. 2a. While this behavior strongly reminds on a typical spin-reorientation transition, extrapolating of the high-field magnetization to zero field does not yield the origin of the graph but gives a finite field value which shows that it is not an ordinary spin-flop transition. To investigate this transition in more detail in particular in the dynamic regime, we measured low-energy spin excitations in this magnetic field range. One of the HF-ESR transmission spectra, measured at $T = 4$ K and a frequency of $f = 708$ GHz, is shown in Fig. 2b. The spectrum features four absorption peaks. The two most prominent resonances ω_1 and ω_{SF} at 25.6 T and 37.4 T are almost symmetric to the spin-flop transition and show similar intensity. An additional sharp but less intense resonance ω_{DM} is observed slightly below the spin-flop field at $B \sim 29.3$ T. The fourth peak ω_{lin} appears at $B_{lin} = 8.1$ T. It shows only weak intensity and belongs to a linear-in-field resonance branch which has an extrapolated zero-field gap of ~ 926 GHz and an effective g -value of $g_{lin} = 1.94$. By removing a thin surface layer of the sample the relative

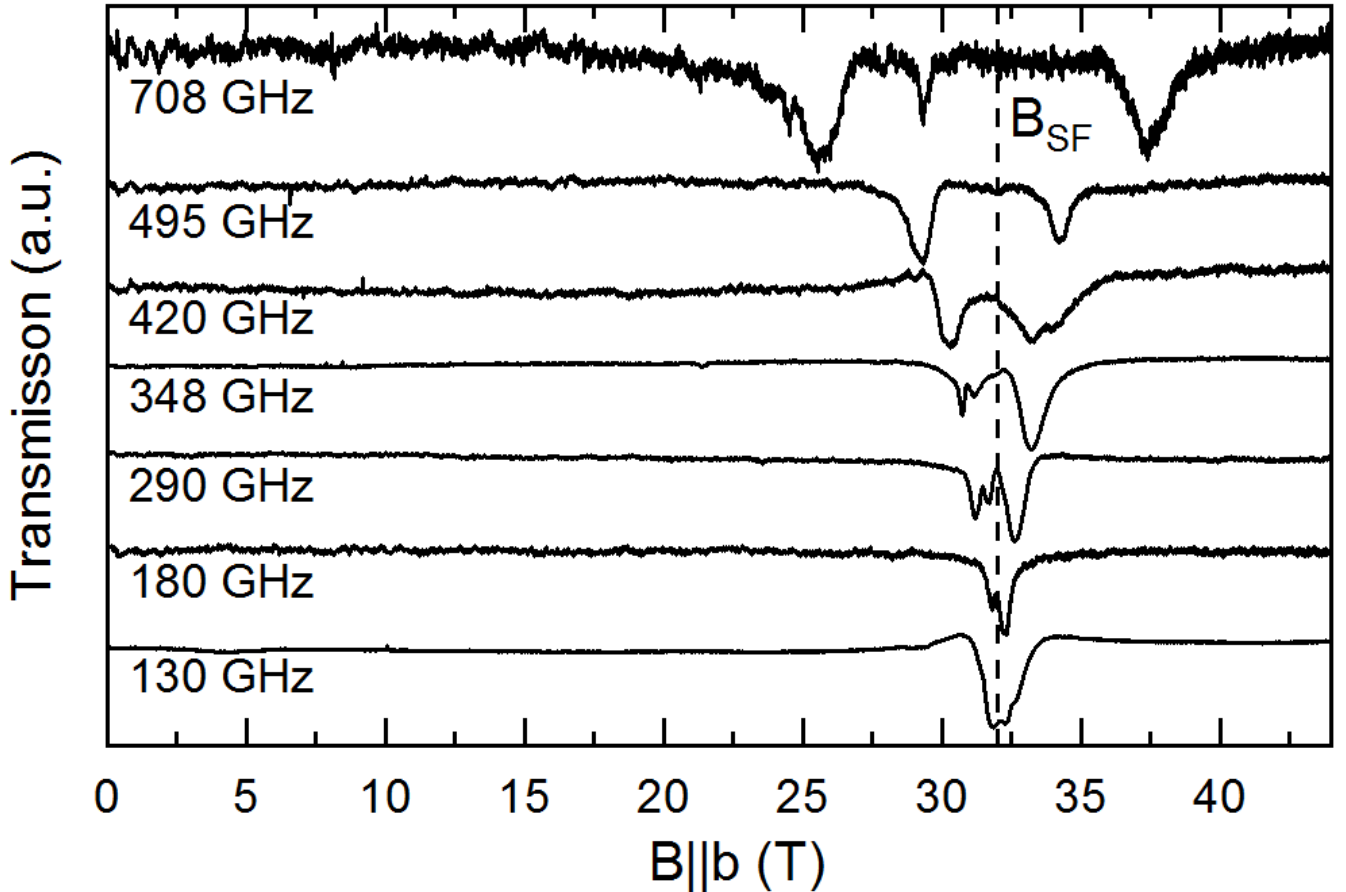


FIG. 3: Pulsed-field electron spin resonance up-sweep transmission spectra at $T \sim 4$ K in the frequency range between $f = 130$ GHz and $f = 708$ GHz. The vertical dashed line indicates the spin-flop field B_{SF} .

intensity of this resonance as compared to the other ones weakens significantly which indicates that it is associated with surface defects.

From inelastic neutron scattering it is known that the magnon excitation gaps at zero field in the Brillouin zone center amount to $\Delta_1 = 1450$ GHz and $\Delta_2 = 2070$ GHz^{15,31,32}. The fact that we observe resonances at 708 GHz as shown in Fig. 2b hence already implies the presence of a resonance branch which is softened by fields $B \parallel b$ -axis. Further progression of softening can be seen in Fig. 3 where the evolution of the resonances at lower frequencies is presented. The data show that splitting of the two main resonance features ω_1 and ω_{SF} shrinks with decreasing frequency and both peaks merge at lowest frequencies under study. At $f = 130$ GHz, only one resonance at the position of the spin-flop field is observed, which indicates complete closing of the excitation gap, i.e., complete softening of the resonance branch. This behaviour is typical for a spin-flop transition which evolves when the external magnetic field compensates the effective field acting on the magnetic sublattice pointing in the direction opposite to the external magnetic field. In addition to softening and merging of the split resonances ω_1 and ω_{SF} , the data show that the resonance ω_{DM} completely vanishes with decreasing frequency and cannot be observed below $f \sim 700$ GHz.

Collecting the resonance fields in a field vs. frequency plot (see Fig. 4) evidences that the magnon gaps not only close but the resonance branches ω_1 and ω_{SF} exhibit a pronounced curvature when approaching B_{SF} . In general, softening of the gaped antiferromagnetic resonance (AFMR) modes is expected but the very strong suppression of the resonance branch is by far not covered by AFMR models^{36,37} with fixed zero-field splittings Δ_1 , Δ_2 and spin-flop field B_{SF} . We recall the large size of Δ_1 as compared to B_{SF} . Specifically, the standard AFMR model would result in the effective g -factor of $g = 3.3(1)$ which is unreasonably large and does not match to $g_b = 2.31$ obtained from analysis of high-temperature magnetic susceptibility data³⁵. Hence, one has to conclude that parameters obtained at zero magnetic field, i.e., single-ion anisotropy D and exchange interaction J , do not describe the experimental results obtained at high magnetic field. The presence of pronounced magnetoelastic effects and associated strong magnetostrictive length changes in LiFePO_4 ³⁵ however already suggests that microscopic parameters are supposed

to be magnetic field dependent. We attribute the apparent failure of the zero-field parameter-based model to field dependence of microscopic parameters and will present an appropriate model in the following.

The spin Hamiltonian presented below extends the one used to describe recent INS data¹⁵ by magnetic fields applied along the b -direction and magnetic field dependent exchange interaction and anisotropy parameters. Specifically, a four magnetic sublattice model is assumed, as indicated in Fig. 1. The sublattices are coupled via the exchange interactions J_{ac} , J_{ab} and J_{bc} . Note, that J_b does not significantly affect the results at $B < B_{\text{SF}}$ and hence is omitted in the Hamiltonian Eq. 1. Interactions along the crystallographic directions are neglected in our model, because these interactions couple one sublattice to itself. In addition to the exchange interactions we add an orthorhombic anisotropy term D as well as Dzyaloshinskii–Moriya (DM) interaction between the sublattices 1-2 and 3-4. As a minimal model to describe the field dependence, for the exchange interactions and the single-ion anisotropy we assume a quadratic magnetic field dependence of the form $J(B) = J(0) \times (1 - \eta B^2)$ and $D(B) = D(0) \times (1 - \iota B^2)$. The Hamiltonian for one unit cell hence reads:

$$\begin{aligned} \mathcal{H} = & 4J_{ac}(S_1 \cdot S_2 + S_3 \cdot S_4) + 4J_{ab}(S_1 \cdot S_3 + S_2 \cdot S_4) \\ & + 4J_{bc}(S_1 \cdot S_4 + S_2 \cdot S_3) + \sum_{i,j} D_i (S_j^i)^2 \\ & + J_{\text{DM}} \cdot (S_1 \times S_2 + S_3 \times S_4) - g\mu_B B \end{aligned} \quad (1)$$

Here, $S^i (i = 1, 2, 3)$, is the i -th component of the sublattice spin S_j ($j = 1..4$), and J_{DM} is the DM interaction.⁴⁷ The value of the g -factor is fixed to $g = 2.31$ as determined from the high-temperature magnetic susceptibility³⁵. To obtain the magnetization along the b -direction, firstly the spin structure is determined by numerically minimizing the Hamiltonian 1 and then the components of the spins in b -direction are calculated. The undetermined parameters in this Hamiltonian are the magnetic field dependencies η , ι and the strength of the DM interaction J_{DM} . The best fitting results for these free parameters to describe the experimental magnetisation data $M(B)||b$ (see Fig. 2) are $\eta = 4.6 \times 10^{-5} \text{ T}^{-2}$, $\iota = 8.0 \times 10^{-5} \text{ T}^{-2}$, and for the DM interaction an upper boundary of $J_{\text{DM}} \leq 0.3 \text{ meV}$ is obtained. Note, that including further terms to the Hamiltonian Eq. (1) or/and assuming higher order terms in the field dependencies of the microscopic parameters will yield quantitative changes while the qualitative scenario of remains robust. Even better fittings can be obtained if a stronger magnetic field dependence, $\eta = 8.1 \times 10^{-5} \text{ T}^{-2}$ and $\iota = 2.6 \times 10^{-4} \text{ T}^{-2}$, for J and D_b are assumed.⁴⁸ However such a strong magnetic field dependence would lead to a change of the easy axis at high fields which is not indicated by the data. We hence restricted the parameter range to small changes of J and D with magnetic fields while excluding strong changes of spin orientation and spin structure. It should be noted, that small DM interactions do not change the spin configuration of the lower-field phase $B < B_{\text{SF}}$. While DM interactions tempt to cant spins of sublattices 1 and 2 with respect to each other, the presence of large anisotropy suppresses canting. In contrast, dynamic response is changed drastically by DM interactions as additional resonances appear.

To simulate the excitations of Hamiltonian 1, the Landau–Lifshitz–Gilbert equation (the spin equation of motion)

$$\frac{dS_j}{dt} = -\frac{\gamma}{1 + \alpha^2} (S_j \times B_{\text{eff},j} + \alpha S_j \times (S_j \times B_{\text{eff},j})) \quad (2)$$

is solved³⁸. It includes the gyromagnetic factor γ and the effective magnetic fields $B_{\text{eff},j}$ acting on the spins of the j -th sublattice. The effective field is composed of the static mean-field and the microwave field. Damping is considered by the parameter α . For the calculations, we chose α sufficiently large to solve the differential equation, but small enough to leave the position of the resonances unchanged within the resolution of the simulation. To match our experiment, the equation of motion (Eq. 2) is solved for unpolarized microwaves in Faraday-geometry. To generate the resonance field vs. frequency diagram, constant frequency cuts are generated and the maxima in absorption are taken as resonance points which reflects the experimental field sweeps.

A simulation of the system, with the best fit parameters of the magnetization measurement and neglecting DM interactions (model 1 in Table I) yields the resonance branches, ω_1 and ω_{SF} , shown in Fig. 4a. While the simulation describes the resonance branch ω_1 below B_{SF} well, it fails to reproduce its behavior in the direct vicinity of the critical field. It also completely misses the presence of the resonance ω_{DM} and fails to reproduce the resonance branch ω_{SF} . Note, that gaps of the resonance branches around B_{SF} are due to sizable mean-fields, which are mainly caused by the fact that the magnetocrystalline anisotropy is large compared to the exchange interactions. In particular, the experimentally observed absence of excitation gaps at B_{SF} is inconsistent with the spin Hamiltonian parameters determined from INS at zero magnetic field. In order to cover the resonance ω_{DM} by the model, DM interaction J_{DM} is introduced, which has been previously suggested to be of finite but small size in zero magnetic field and was hence neglected in the simulation of the spin dynamics probed by INS^{15,32}. The best simulation, which takes into

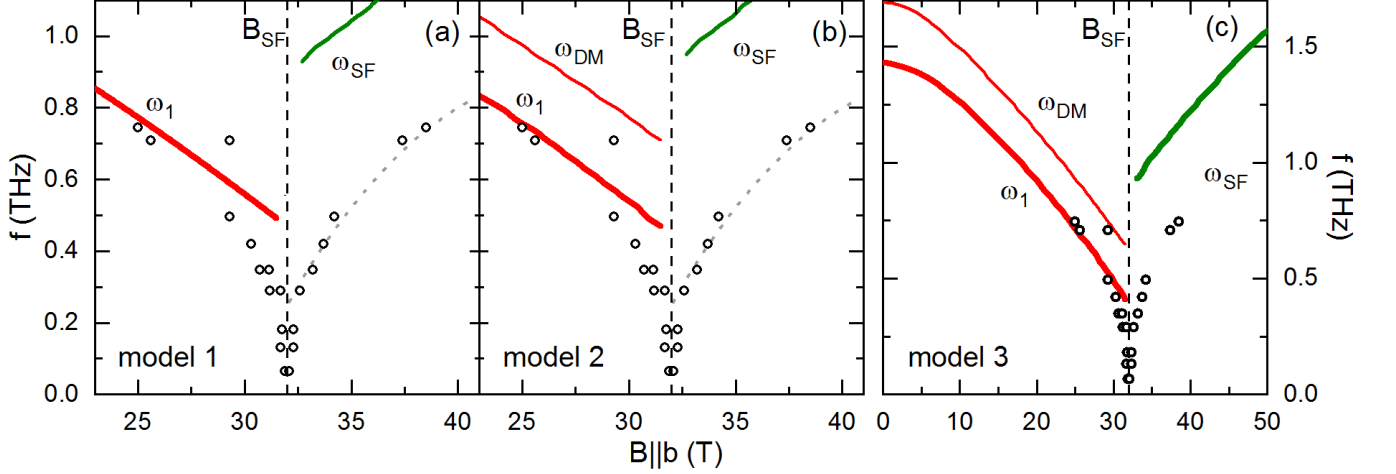


FIG. 4: Resonance fields at different frequencies (data points, cf. Fig. 3). Vertical dashed lines indicate the spin-flop field, gray dotted lines are guide to the eye. Solid lines are model calculations with (a) exchange interactions J and anisotropy D_b being magnetic field-dependent parameters (Model 1), (b) with additional Dzyaloshinskii–Moriya interaction (Model 2), and (c) with a magnetic field dependent anisotropy tensor D (Model 3). See Table I for simulation parameters and Fig. S1 (Supplemental Material) for a further comparison of the models.

	Model 1	Model 2	Model 3
D_a	$0.62 \times r_2(B)$	$0.62 \times r_2(B)$	$0.62 \times r_2(B)$
D_c	1.56	1.56	$1.56 \times r_3(B)$
J_{bc}	$0.77 \times r_1(B)$	$0.77 \times r_1(B)$	$0.77 \times r_1(B)$
J_{ab}	$0.14 \times r_1(B)$	$0.14 \times r_1(B)$	$0.14 \times r_1(B)$
J_{ac}	$0.05 \times r_1(B)$	$0.05 \times r_1(B)$	$0.05 \times r_1(B)$
J_{DM}	0	0.15	0.15

TABLE I: Simulation parameters in units of meV for the three used models. The magnetic field dependence is marked by $r_{2,3}(B)$ and $r_1(B)$ for the anisotropy and exchange interaction, respectively. The magnetic field dependencies are given by $r_1 = 1 - 4.6 \times 10^{-5} B^2/T^2$, $r_2 = 1 - 8.0 \times 10^{-5} B^2/T^2$ and $r_3 = 1 - 1.7 \times 10^{-4} B^2/T^2$.

account the position of ω_{DM} as well as the ratio of intensities of ω_1 and ω_{DM} is achieved by $J_{DM} = 0.15$ meV (see Table I model 2). As shown in Fig. 4b, considering the DM term indeed yields both the resonance branches ω_1 and ω_{DM} . Similar to model 1, the simulated results however differ from the experimental data in the vicinity of B_{SF} . In the flopped phase no additional resonance is observed, however the resonance branch ω_{SF} is slightly shifted to higher energies as compared to model 1.

In order to further improve the model by employing field dependent microscopic parameters, we introduce magnetic field dependence of D_c (see Table I model 3). Magnetic field $B||b$ -dependence of D_c with $D_c(B) > D_a(B)$ does not change the simulated magnetisation shown in 2, because for small DM interactions and $B||b$ the spins are confined to the ab -plane. In addition, also ω_1 and ω_{DM} are only affected insignificantly for fields well below B_{SF} . While, there are clear changes around the spin-flop transition leading a good description of the modes in this field range, too. We obtain the magnetic field dependence $\iota_2 = 1.7 \times 10^{-4} \text{ T}^{-2}$ of $D_c(B)$ which was derived by restricting $D_a(B) < D_c(B)$ for all magnetic fields.

Transmission spectra at a fixed frequency, presented in Fig. 5, show the dependence of the resonances discussed above upon increasing the temperature. At $T = 2.6$ K the resonances ω_1 and ω_{SF} are visible. The resonance ω_1 shows an additional splitting at this temperature. With increasing temperature the intensity of the peaks diminishes. While the position and half width of ω_1 do not significantly change upon heating, the resonance ω_{SF} shifts with temperature to higher fields and broadens significantly. At $T \approx 16$ K the resonance ω_1 has completely vanished while ω_{SF} remains as a broad feature similar to a feature at B_{SF} . At $T = 20$ K, no resonance is observed up to $B = 45$ T.

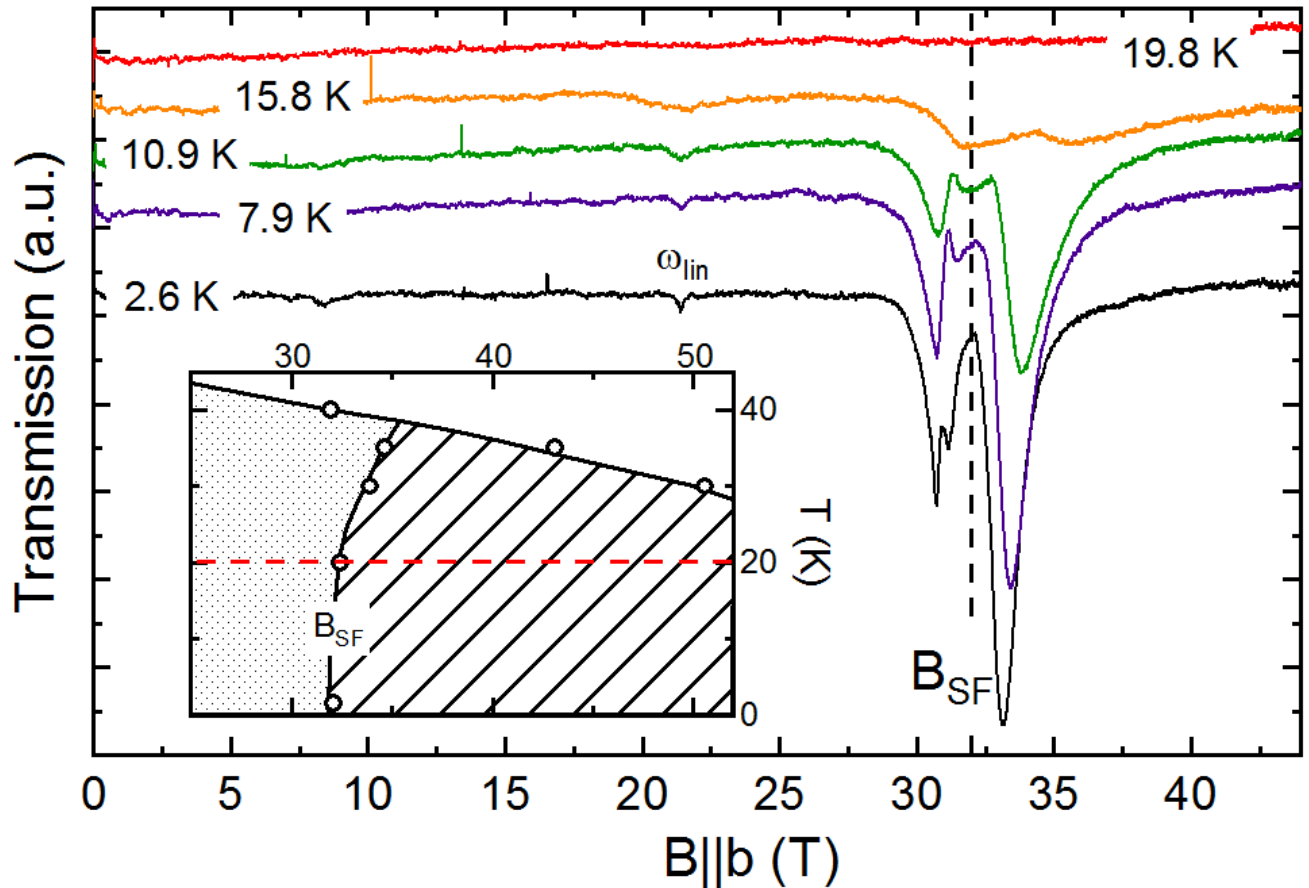


FIG. 5: HF-ESR transmission spectra measured at $f = 348$ GHz in the temperature regime between 2.6 K and ~ 20 K. The vertical dashed line indicates the spin-flop field. Inset shows the magnetic phase diagram of LiFePO_4 , data from Ref. [35]. The horizontal dashed (red) line marks the position, where the $T = 19.8$ K spectrum was measured.

IV. DISCUSSION

The experimental data are well described by the used models for magnetic field $B \leq B_{\text{SF}}$. In particular, the presence of sizable DM interaction is evidenced by the presence of ω_{DM} . Introducing magnetic field-dependent parameters yields an excellent description of the field dependence of AFMR modes and resolves the quantitative contradiction between zero-field gap as detected by INS and the actual value of B_{SF} . To be specific, the extended model shown in Fig. 4 reproduces both the experimentally observed ω_1 and ω_{DM} resonance features and the bending on the former when approaching B_{SF} . The field-dependence of microscopic parameters is motivated by the presence of pronounced magnetostrictive effects in LiFePO_4 ³⁵. While the presence of DM interaction was suggested recently, it has neither been directly evidenced experimentally yet nor quantified in the dynamic response probed by INS^{15,32}. Analysis of our high-field ESR data yields $J_{\text{DM}} \approx 150 \mu\text{eV}$. Note, that this value can not straightforwardly extrapolated to zero magnetic field as our analysis implies the above mentioned field dependence of spin Hamiltonian parameters. In contrast to excellent description of the AFMR modes below B_{SF} , all applied models fail to quantitatively reproduce the observed resonances above B_{SF} . One may speculate that the spin structure in the high-field phase is not a purely reoriented one but further differs from the ground state. In addition, the spin-flop transition might be accompanied by structural distortions. Such distortions could change the anisotropy or the exchange interactions not in the continuous manner, assumed here, but rather abruptly. This is somehow corroborated by the fact that the spectra presented in Fig. 5 indeed show that the resonances below and above B_{SF} are clearly different regarding the spectral weight. In addition, while, at $f = 348$ GHz, ω_1 does not shift upon heating, there is a clear temperature dependence of ω_{SF} which shifts to higher fields. This suggests a decrease of internal fields upon heating while for $B < B_{\text{SF}}$ constant internal mean-fields are evidenced. Notably, in contrast to our experimental findings, conventional mean-field theory would suggest a shift of ω_{SF} to lower fields upon heating³⁷. We also note that rather large modulations of exchange

interactions or anisotropy at phase boundaries and resulting changes in the magnon spectra have been previously observed by HF-ESR in other compounds, e.g. in HgCr_2O_4 ³⁹, CuFeO_2 ⁴⁰, CdCr_2O_4 ⁴¹, or $\text{Cu}(\text{pz})_2(\text{ClO}_4)_2$ ⁴².

The disappearance of the resonances at $T = 20$ K is somehow surprising, because the measurement takes place well in the long-range antiferromagnetically ordered phase as illustrated by the dashed red line in the phase diagram (see the inset of Fig. 5). Specifically, the phase diagram indicates no phase transition or any feature separating a region where AFMR modes are detected in the vicinity of B_{SF} (i.e., below the dashed line in the inset of Fig. 5) from the one without observable features. We recall that the antiferromagnetic order parameter in LiFePO_4 is only very weakly temperature dependent up to 20 K and it only marginally depends on small fields in related materials LiMnPO_4 and LiCoPO_4 ^{15,27,31,43,44}. We also note that there are only very small changes of the magnetisation between 1.5 K and 20 K at any given field up to $B = 50$ T, i.e., the uniform susceptibility $\chi(\omega = 0) = \partial M / \partial B$ is rather constant in this temperature and field range. Note, however, that the slope of the phase boundary $B_{\text{SF}}(T)$ starts to increase above 20 K which may indicate that the presence of fluctuations or of competing interactions is associated with the disappearance of the AFMR resonances. From an experimental point of view, there are two obvious reasons which can lead to no observable resonance at $f = 348$ GHz. These are (1) enormous broadening, leading to resonances indistinguishable from the background and (2) shift of the resonance branches above the measured frequency regime. Following the tendency of spectra up to 16 K, both options are very unlikely. Alternatively, one may consider excitations which change the length of the spin, which is in our model constant. In Ref. 32 such resonances, there called hybrid excitations, are found by inelastic neutron scattering at $\Delta = 1088$ GHz in zero magnetic field. If such excitations exist, a spectral shift of intensity from the conventional magnon excitations to spin stretching modes could take place at higher temperatures around the spin-flop transition. However, our ESR data do not show any sign of such hybrid excitation.

In order to further clarify the magnetic field dependence of anisotropy parameters and DM interaction, measurements in the terahertz regime will be needed. We hence suggest to study the resonance branch ω_2 which exhibits zero field splitting of $\Delta_2 = 2070$ GHz³², as this branch is particularly sensitive to changes of D_c . While, below ≈ 25 T, ω_1 only weakly depends on D_c as shown in Fig. 4c, the slope of ω_2 is significantly affected. Recent THz-absorption spectroscopy data on other olivine-structured phosphates show divers behavior. In LiCoPO_4 , two modes are observed in zero magnetic fields which split into four modes upon application of magnetic field along the easy axis, two of which being suppressed and two stabilised in the fields^{28,29}. All four branches show rather linear field dependence of similar absolute slope, i.e., similar effective g -factor. In contrast, low-lying excitation branches in LiNiPO_4 are non-linear already at relatively small magnetic fields applied along the easy magnetic axis²³.

We finally note that our bare experimental data do not unambiguously tell whether the observed modes are classical antiferromagnetic resonances, i.e., whether they are only magnetic dipole active, or whether they are electromagnons and can be excited by oscillating electrical fields, too. As illustrated, e.g., by the example of multiferroic TbMnO_3 , electromagnons and antiferromagnetic resonances can coexist⁴⁵ which in principle cannot be excluded for LiFePO_4 in magnetic fields, either. However, the magnetic structure of LiFePO_4 implies at least two AFMR branches which presence at zero field was confirmed by INS. Attributing ω_1 to AFMR is further corroborated by the fact that ω_1 follows the magnetisation which is expected for an antiferromagnetic resonance. In addition, the magnetoelectric effect is comparably small in LiFePO_4 and there is no electric order which further motivates attributing the observed modes to the expected AFMR ones.

A. Summary

We report antiferromagnetic magnon excitations in LiFePO_4 in high fields around the spin flop transition. The data reveal closing of the energy gap exactly at B_{SF} and hardening the AFMR modes for higher fields. An additional mode below B_{SF} is assigned to DM interaction which size is estimated to $150\mu\text{eV}$. The mean-field theory model obtained from previous zero-field INS data only describes the field dependence of the magnon modes and of the magnetisation if exchange interactions and magnetocrystalline anisotropy are considered to change with magnetic field. This also holds for the value of the spin-flop field. The AFMR modes disappear at around 20 K, i.e., well in the long-range AFM ordered phase, which might suggest the presence of spin fluctuations or competing interactions.

Acknowledgments

The project is supported by Deutsche Forschungsgemeinschaft (DFG) through KL 1824/13-1 and the Heidelberg STRUCTURES Excellence Cluster (EXC2181/1-390900948). Funding by BMBF via project SpinFun (project 13XP5088) is gratefully acknowledged. We acknowledge the support of the HLD at HZDR, member of the European

Magnetic Field Laboratory (EMFL). S.Z. and A.P. acknowledge the support of DFG through ZV 6/2-2.

-
- * Email: klingeler@kip.uni-heidelberg.de
- ¹ J. Jeong, E. Goremychkin, T. Guidi, K. Nakajima, G. S. Jeon, S.-A. Kim, S. Furukawa, Y. B. Kim, S. Lee, V. Kiryukhin, et al., *Physical Review Letters* **108**, 077202 (2012).
 - ² M. Matsuda, R. S. Fishman, T. Hong, C. Lee, T. Ushiyama, Y. Yanagisawa, Y. Tomioka, and T. Ito, *Physical Review Letters* **109**, 067205 (2012).
 - ³ Z. Xu, J. Wen, T. Berlijn, P. M. Gehring, C. Stock, M. B. Stone, W. Ku, G. Gu, S. M. Shapiro, R. Birgeneau, et al., *Physical Review B* **86**, 174419 (2012).
 - ⁴ D. Talbayev, S. Trugman, S. Lee, H. T. Yi, S.-W. Cheong, and A. Taylor, *Physical Review B* **83**, 094403 (2011).
 - ⁵ U. Nagel, R. S. Fishman, T. Katuwal, H. Engelkamp, D. Talbayev, H. T. Yi, S.-W. Cheong, and T. Rõõm, *Physical Review Letters* **110**, 257201 (2013).
 - ⁶ R. S. Fishman, J. H. Lee, S. Bordács, I. Kézsmárki, U. Nagel, and T. Room, *Physical Review B* **92**, 094422 (2015).
 - ⁷ B. Ruetter, S. Zvyagin, A. P. Pyatakov, A. Bush, J. Li, V. Belotelov, A. Zvezdin, and D. Viehland, *Physical Review B* **69**, 064114 (2004).
 - ⁸ M. Cazayous, Y. Gallais, A. Sacuto, R. De Sousa, D. Lebeugle, and D. Colson, *Physical Review Letters* **101**, 037601 (2008).
 - ⁹ P. Rovillain, R. De Sousa, Y. Gallais, A. Sacuto, M. Méasson, D. Colson, A. Forget, M. Bibes, A. Barthélémy, and M. Cazayous, *Nature materials* **9**, 975 (2010).
 - ¹⁰ A. S. Zimmermann, B. B. Van Aken, H. Schmid, J.-P. Rivera, J. Li, D. Vaknin, and M. Fiebig, *The European Physical Journal B* **71**, 355 (2009).
 - ¹¹ J.-P. Rivera, *Ferroelectrics* **161**, 147 (1994).
 - ¹² B. B. Van Aken, J.-P. Rivera, H. Schmid, and M. Fiebig, *Physical Review Letters* **101**, 157202 (2008).
 - ¹³ B. B. Van Aken, J.-P. Rivera, H. Schmid, and M. Fiebig, *Nature* **449**, 702 (2007).
 - ¹⁴ D. Vaknin, J. L. Zarestky, J.-P. Rivera, and H. Schmid, *Physical Review Letters* **92**, 207201 (2004).
 - ¹⁵ R. Toft-Petersen, M. Reehuis, T. B. Jensen, N. H. Andersen, J. Li, M. D. Le, M. Laver, C. Niedermayer, B. Klemke, K. Lefmann, et al., *Physical Review B* **92**, 024404 (2015).
 - ¹⁶ D. Arčon, A. Zorko, P. Cevc, R. Dominko, M. Bele, J. Jamnik, Z. Jagličić, and I. Golosovsky, *Journal of Physics and Chemistry of Solids* **65**, 1773 (2004).
 - ¹⁷ J. Li, W. Tian, Y. Chen, J. L. Zarestky, J. W. Lynn, and D. Vaknin, *Physical Review B* **79**, 144410 (2009).
 - ¹⁸ C. Calderon Filho, P. Gomes, A. García-Flores, G. Barberis, and E. Granado, *Journal of Magnetism and Magnetic Materials* **377**, 430 (2015).
 - ¹⁹ V. Fomin, V. Gnezdilov, V. Kurnosov, A. Peschanskii, A. Yermenko, H. Schmid, J.-P. Rivera, and S. Gentil, *Low Temperature Physics* **28**, 203 (2002).
 - ²⁰ T. B. S. Jensen, N. B. Christensen, M. Kenzelmann, H. Rønnow, C. Niedermayer, N. H. Andersen, K. Lefmann, M. Jiménez-Ruiz, F. Demmel, J. Li, et al., *Physical Review B* **79**, 092413 (2009).
 - ²¹ R. Toft-Petersen, J. Jensen, T. B. S. Jensen, N. H. Andersen, N. B. Christensen, C. Niedermayer, M. Kenzelmann, M. Skoulatos, M. D. Le, K. Lefmann, et al., *Physical Review B* **84**, 054408 (2011).
 - ²² J. Li, T. B. Jensen, N. H. Andersen, J. L. Zarestky, R. W. McCallum, J.-H. Chung, J. W. Lynn, and D. Vaknin, *Physical Review B* **79**, 174435 (2009).
 - ²³ L. Peedu, V. Kocsis, D. Szaller, J. Viirok, U. Nagel, T. Rõõm, D. G. Farkas, S. Bordács, D. Kamenskyi, U. Zeitler, et al., *Physical Review B* **100**, 024406 (2019).
 - ²⁴ D. Rigitano, D. Vaknin, G. Barberis, and E. Granado, *Physical Review B* **101**, 024417 (2020).
 - ²⁵ D. Vaknin, J. Zarestky, L. Miller, J.-P. Rivera, and H. Schmid, *Physical Review B* **65**, 224414 (2002).
 - ²⁶ W. Tian, J. Li, J. W. Lynn, J. L. Zarestky, and D. Vaknin, *Physical Review B* **78**, 184429 (2008).
 - ²⁷ W. Tian, J. Li, H. Li, J. W. Lynn, J. L. Zarestky, and D. Vaknin, *Journal of Physics: Conference Series* **251**, 012005 (2010).
 - ²⁸ V. Kocsis, S. Bordács, Y. Tokunaga, J. Viirok, L. Peedu, T. Rõõm, U. Nagel, Y. Taguchi, Y. Tokura, and I. Kézsmárki, *Physical Review B* **100**, 155124 (2019).
 - ²⁹ V. Kocsis, K. Penc, T. Rõõm, U. Nagel, J. Vít, J. Romhányi, Y. Tokunaga, Y. Taguchi, Y. Tokura, I. Kézsmárki, et al., *Physical Review Letters* **121**, 057601 (2018).
 - ³⁰ W. Paraguassu, P. Freire, V. Lemos, S. Lala, L. Montoro, and J. M. Rosolen, *Journal of Raman Spectroscopy: An International Journal for Original Work in all Aspects of Raman Spectroscopy, Including Higher Order Processes, and also Brillouin and Rayleigh Scattering* **36**, 213 (2005).
 - ³¹ J. Li, V. O. Garlea, J. L. Zarestky, and D. Vaknin, *Physical Review B* **73**, 024410 (2006).
 - ³² Y. Yiu, M. D. Le, R. Toft-Petersen, G. Ehlers, R. J. McQueeney, and D. Vaknin, *Physical Review B* **95**, 104409 (2017).
 - ³³ K. Momma and F. Izumi, *Journal of Applied Crystallography* **44**, 1272 (2011).
 - ³⁴ C. Neef, H. Wadepohl, H.-P. Meyer, and R. Klingeler, *Journal of Crystal Growth* **462**, 50 (2017).
 - ³⁵ J. Werner, S. Sauerland, C. Koo, C. Neef, A. Pollithy, Y. Skourski, and R. Klingeler, *Physical Review B* **99**, 214432 (2019).
 - ³⁶ T. Nagamiya, *Progress of Theoretical Physics* **6**, 342 (1951).
 - ³⁷ T. Nagamiya, *Progress of Theoretical Physics* **11**, 309 (1954).
 - ³⁸ B. Hillebrands and K. Ounadjela, *Spin dynamics in confined magnetic structures I*, vol. 83 (Springer Science & Business

Media, 2003).

- ³⁹ S. Kimura, M. Hagiwara, T. Takeuchi, H. Yamaguchi, H. Ueda, Y. Ueda, and K. Kindo, *Physical Review B* **83**, 214401 (2011).
- ⁴⁰ S. Kimura, T. Fujita, N. Nishihagi, H. Yamaguchi, T. Kashiwagi, M. Hagiwara, N. Terada, Y. Sawai, and K. Kindo, *Physical Review B* **84**, 104449 (2011).
- ⁴¹ S. Kimura, Y. Sawada, Y. Narumi, K. Watanabe, M. Hagiwara, K. Kindo, and H. Ueda, *Physical Review B* **92**, 144410 (2015).
- ⁴² K. Y. Povarov, A. I. Smirnov, and C. P. Landee, *Physical Review B* **87**, 214402 (2013).
- ⁴³ R. Toft-Petersen, N. H. Andersen, H. Li, J. Li, W. Tian, S. L. Bud'ko, T. B. Jensen, C. Niedermayer, M. Laver, O. Zaharko, et al., *Physical Review B* **85**, 224415 (2012).
- ⁴⁴ E. Fogh, R. Toft-Petersen, E. Ressouche, C. Niedermayer, S. L. Holm, M. Bartkowiak, O. Prokhnenko, S. Sloth, F. W. Isaksen, D. Vaknin, et al., *Physical Review B* **96**, 104420 (2017).
- ⁴⁵ A. Pimenov, A. Shuvaev, A. Loidl, F. Schrettle, A. Mukhin, V. Travkin, V. Y. Ivanov, and A. Balbashov, *Physical Review Letters* **102**, 107203 (2009).
- ⁴⁶ Note, that J_b does not significantly affect the AFMR model at $B < B_{SF}$ and hence is omitted in the Hamiltonian Eq. 1.
- ⁴⁷ S is the thermal average of the spin, so that the magnetisation reads $M = g\mu_B S$.
- ⁴⁸ The resulting field dependencies quantitatively depend on the actual microscopic parameters at $B = 0$ T which are taken from Ref.¹⁵.